

**Title: Epigenetic Changes Accompany Developmental Programmed Cell Death
In Tapetum Cells**

Running head: Epigenetic changes during tapetum PCD

María-Teresa Solís¹, Nandini Chakrabarti^{1,a}, Eduardo Corredor^{1,a}, Josefina Cortés-Eslava^{1,2}, María Rodríguez-Serrano¹, Marco Biggiogera³, María C. Risueño¹,
Pilar S. Testillano^{1,*}

¹Pollen Biotechnology of Crop Plants group. Biological Research Center, CIB, CSIC.
Ramiro de Maeztu 9, 28040 Madrid, Spain.

² Instituto de Ciencias de la Atmósfera, UNAM, Dep. Ciencias Ambientales
Ciudad Universitaria de Coyoacán, México DF, 04510 México.

³ Laboratorio di Biologia Cellulare e Neurobiologia, Dipartimento di Biologia Animale,
Universita di Pavia and Istituto di Genetica Molecolare del CNR, Piazza Botta 10, 27100,
Pavia, Italy.

^aBoth authors contributed equally to this work.

*Corresponding author

Abbreviations:

PCD: programmed cell death, MET1: DNA methyl transferase 1, HERDS: heterogeneous ectopic ribonucleoprotein-derived structures.

Footnote:

Present address of María Rodríguez-Serrano: EEZ, CSIC, Granada, Spain

ABSTRACT

The tapetum, nursing tissue inside anthers undergoes cellular degradation by programmed cell death (PCD) during late stages of microspore-early pollen development. Despite the key function of tapetum, little is known about the molecular mechanisms regulating this cell death process in which profound nuclear and chromatin changes occur. Epigenetic features (DNA methylation and histone modifications), have been revealed as hallmarks that establish the functional status of chromatin domains, but no evidences on the epigenetic regulation of PCD have been reported. DNA methylation is accomplished by DNA methyltransferases, among them, MET1 constitutes one of the CG maintenance methyltransferase in plants, also showing *de novo* methyltransferase activity

In this work, the changes in epigenetic marks during the PCD of tapetal cells has been investigated by a multidisciplinary approach to reveal the dynamics of DNA methylation and the pattern of expression of *MET1* DNA methyltransferase in relation to the main cellular changes of this PCD process which have been also characterized in two species, *Brassica napus* and *Nicotiana tabacum*.

Results showed that tapetum PCD progresses with the increase in global DNA methylation and *MET1* expression, epigenetic changes that accompanied reorganization of the nuclear architecture and a high chromatin condensation, activity of caspase 3-like proteases, and cytochrome C release. The reported data indicates a relation between the PCD process and the DNA methylation dynamics and *MET1* expression in tapetal cells, suggesting a possible new role of the epigenetic marks in the nuclear events occurring during this cell death process and giving new insights in the knowledge of the epigenetic control of plant PCD.

Key words: Anther development, DNA methylation, DNA methyltransferase, 5-methyl-deoxy-cytosine, *Brassica napus*, *Nicotiana tabacum*.

INTRODUCTION

Male reproductive development in higher plants is a complex biological process involving the correlated differentiation of anther tissues and the generation of haploid microspores and pollen grains. The developing anther consists on the microsporocytes at the center, surrounded by the tapetum and the anther wall with three somatic layers: the exothecium, the endothecium and the middle layer (Goldberg et al. 1993, Feng and Dickinson 2010). The tapetum is originated at the last division of the sporogeneous tissue that forms the microsporocytes and the tapetal cells (Feng and Dickinson 2010), which directly contact with the microspore mother cells. They undergo meiosis to give arise the microspore tetrads. The tapetum plays a crucial role in the microspore and early pollen formation, after the asymmetric division, as nutritive and secretory tissue involved in the formation of the exine, the pollen wall, (Risueño et al. 1969, Li et al. 2006, Parish and Li 2010). As a secretory cell layer, the tapetum also provides enzymes for the release of microspores from their special callose wall at the tetrad stage, and components to the pollen wall layers (Testillano et al. 1993). It is known that the tapetum undergoes cellular degradation during late stages of microspore development (Vardar and Unal 2012). This degradation process is considered to be a programmed cell death (PCD) event (Papini et al. 1999, Wu and Cheung 2000), but little is known about the cellular and molecular mechanisms regulating this PCD process.

Programmed cell death (PCD) is a genetically controlled process that occurs both in animal and plant cells (Wu and Cheung 2000, Wang et al. 2009, Coll et al. 2011). It plays a fundamental role during normal development and in various processes like: the response to stress, including that caused by pathogenic infection (Collazo et al. 2006), the leaf senescence, the removal of aleurone cells and root cap cells and the xylogenesis (Rogers 2006). PCD is also of special importance for plant reproduction, during embryo development, anther dehiscence, pollen germination and pollen tube growth, pistil development, and pollen-pistil interactions (Wu and Cheung 2000). Different pathways of PCD can be found in plants: necrotic, autophagic and apoptotic-like (Kacprzyk et al. 2011), the apoptotic-like type characterized by typical apoptotic-like features (Reape and McCabe 2008, Reape and McCabe 2010, Tewari et al. 2012). This apoptotic-like plant PCD includes mitochondrial changes and release of cytochrome C to the cytoplasm (Wu

and Cheung 2000, Balk and Leaver 2001, Vacca et al. 2006) and chromatin condensation paralleled by DNA fragmentation; these events are some of the most important phenomena occurring during the most common PCD pathway in animals, the apoptosis (Fullgrabe et al. 2010). The apoptotic pathway in animals is characterized by the activity of caspases, key executor proteases of the death program (Lam 2004). Although there are no close sequences homologues of classical caspases in the plant genome, evidence of enzymatic activity, such as that of caspase 3-like proteases, has also been reported in different plant systems undergoing PCD processes, including that involved in the rejection of incompatible pollen (Thomas and Franklin-Tong 2004, Bosch and Franklin-Tong 2007, Reape and McCabe 2008, Wang et al. 2009), but no data on the caspase-like activities in tapetum PCD has been reported until now. Several types of proteolytic activities have been recently identified as taken part in tapetum PCD in different species, among them, aspartic proteases have been reported to play a critical role in this process (Parish and Li 2010, Phan et al. 2011, Phan et al. 2012, Niu et al. 2013).

DNA methylation and histone modifications have been revealed as hallmarks that establish the functional status of chromatin domains (Tessadori et al. 2004) and confer the flexibility of transcriptional regulation necessary for plant development and adaptive responses to the environment (Grant-Downton and Dickinson 2005, Vaillant and Paszkowski 2007). There is a great deal of evidence pointing to the idea that the major effect of methyl groups in cytosines is to model chromatin structure at different levels, although the precise mechanisms by which DNA methylation affects chromatin packaging have not been completely elucidated (Cedar and Bergman 2012). DNA methylation of cytosine residues is accomplished by DNA methyltransferases, which can transfer methyl groups from S-adenosylmethionine to the DNA. DNA methyltransferase 1 (MET1) has been reported as the CG maintenance methyltransferase in plants, based on sequence similarity to Dnmt1, the orthologous mammalian maintenance methyltransferase. However, there are increasing evidences suggesting that MET1 might also have *de novo* methyltransferase activity (Gehring and Henikoff 2007, Solís et al. 2012). Epigenetic features are likely to have a major role in the regulation of the nuclear changes experienced by apoptotic-like cells, but no evidences on the epigenetic regulation of PCD have been reported.

In this work, the dynamics of DNA methylation during PCD of tapetal cells and its relation to key apoptotic-like features have been characterized by a multidisciplinary approach. Firstly, the main subcellular rearrangements and apoptotic-like features, including nuclear and chromatin structural changes, cytochrome C release and caspase 3-like activity, have been analyzed during tapetum PCD in two different plant species, *Brassica napus* and *Nicotiana tabacum*. Secondly, the dynamics of DNA methylation patterns in relation to nuclear changes, and the expression of *MET1* DNA methyltransferase have been characterized during tapetum PCD. Results showed, in both plant species studied, that tapetum PCD is accompanied by epigenetic changes, specifically by an increase in DNA methylation and *MET1* gene expression, together with the reorganization of the nuclear domains architecture, high chromatin condensation, fragmentation of the nucleolus and RNP segregation, activity of caspase 3-like proteases and cytochrome C release. Taken together, these data give new insights in the knowledge of the epigenetic control of PCD processes.

RESULTS

Characterization of main subcellular changes during tapetum PCD

The first step of the study was the selection of the most representative stages of tapetum development to be processed and analyzed. Anthers from different bud sizes were collected to monitor the tapetum programmed cell death (PCD) process that accompanies microsporogenesis and early pollen development. Three main tapetum developmental stages were selected and named as: “active tapetum”, “tapetum at PCD” and “tapetum at late PCD”. Structural changes were studied in semithin sections which were either stained by toluidine blue or subjected to RNA immunofluorescence to analyze cytoplasmic RNA content and distribution. Electron microscopy (EM) analysis was also performed to reveal specific ultrastructural features.

“Active tapetum stage” corresponded with a long stage starting with the microsporocyte at the meiotic prophase stage and finishing with the initiation of tapetum PCD. At this stage tapetum cells presented a large size with rectangular shape and large rounded nuclei (Fig. 1A, arrows) with a chromatin pattern in network threads of different sizes, as revealed by EM (Fig. 2A, 2B); they showed dense cytoplasm with abundant ribosomes detected by anti-RNA immunofluorescence (Fig. 1A, 1B) indicative feature of very active cells to accomplish both, nutritive and secretory functions. Later in development, at the early vacuolated microspore stage, tapetum cells showed initial features of PCD: they lost their geometrical shape and presented elongated nuclei (Fig. 1C, arrow, 2C, 2D) and fragmented nucleolus (Fig. 2C, 2D). This stage was selected and named as “tapetum at PCD”. The chromatin appeared more condensed forming irregular and large chromatin masses, the nucleus became compacted and lobulated (Fig. 1C, 2C) and the nucleolus fragmented (Fig. 2D, arrows). The RNA immunofluorescence signal at this stage was still present in cytoplasmic areas of tapetum and microspores (Fig. 1D), whereas very low or absent RNA signal was observed in anther cell layers behind the tapetum (Fig. 1D, AW) due to the high vacuolation and the very thin layer of cytoplasm present in these cells. As development progressed, at early pollen stage, tapetum cells became degraded till to disappear, the nuclear remnants displayed much smaller size and lobular or elongated shape (Fig. 1E, arrow) with high condensed chromatin (Fig. 1E, 1F). This stage was selected and named as “tapetum at late PCD”. The tapetal cells showed irregular shapes and organization (Fig. 1E, 2E), their cytoplasm presented very low levels

of RNA, as revealed by the decrease of anti-RNA immunofluorescence signal (Fig.1F), indicating a massive ribosomes and transcripts degradation at this stage. Anther cell layers behind the tapetum were highly vacuolated at this stage, and did not show detectable RNA signal (Fig. 1E, 1F, AW).

Electron microscopy analysis revealed specific ultrastructural features during PCD. In *Brassica napus*, in the “active tapetum” stage, the nucleus appeared spherical with a relatively centered large nucleolus (Fig. 2A, 2B, arrow), a wide interchromatin region plenty of fibrillo-granular RNP structures, and small masses of condensed chromatin (Fig. 2A, 2B). Later, in “tapetum at PCD” stage, the cytoplasmic and nuclear compartments have lost their normal architecture and some new structural rearrangements were observed. Chromatin progressively condensed and heterochromatin masses occupied much larger nuclear regions, the nucleus exhibited invaginations (Fig. 2C, arrow) and an elongated and narrow shape (Fig. 2C, 2D), RNP structures of the interchromatin region aggregated and segregated from chromatin territories and nucleolus fragmented in several nucleolar bodies (arrows in Fig. 2D). At “late PCD” stages (Fig. 2E), nuclei were highly fragmented, the presence of RNPs clusters increased, and new dense structures of approximately 0.2 μm size and positives to the EDTA staining preferential for RNPs were observed in the cytoplasm (Fig. 2F, arrows); these structures, not reported in plant cells yet, resembled to the heterogeneous ectopic RNP-derived structures (HERDS), of apoptotic animal cells (Biggiogera and Pellicciari 2000). These RNP structures will be also named as HERDS to indicate all those RNP-containing heterogeneous structures observed outside their nuclear locations at late PCD in the two species of our study, *Brassica napus* and *Nicotiana tabacum* (data not shown).

Cytochrome C was localized in the tapetum by immunofluorescence using monoclonal antibodies at the developmental stages of “active tapetum” and “tapetum at PCD” to analyze whether cytochrome C release to the cytoplasms occurred in the tapetal cells of the species under study. Since cytochrome C release is an early event during the PCD process (Balk and Leaver 2001) no later developmental stages were used for this immunolocalization. The specificity of the antibody was demonstrated by western blotting assay on total protein extracts obtained from anthers. Western results showed that the antibody recognized a band of 15kDa corresponding to the known cytochrome C molecular weight, in the two developmental stages analyzed (Fig. 3A), assessing the specificity of the

immunofluorescence results. Anti-cytochrome C immunofluorescence assays were analyzed under confocal microscopy using the same laser excitation and sample emission capture settings for image acquisition in all immunofluorescence preparations, this procedure permitted an accurate and reliable comparison between signals from cells at different developmental stages. Results revealed a punctate fluorescent signal in the cytoplasm of “active tapetum” cells corresponding to the mitochondria (Fig 3B, 3B’, 3D, 3D’), while at the beginning of the PCD process tapetum cells exhibited, together with the punctate pattern, a faint diffuse fluorescent signal in their cytoplasm (Fig. 3C, 3C’, 3E, 3E’) indicating the partial release of cytochrome C molecules to the cytoplasm. Similar results were obtained in both *B. napus* (Fig. 3B, 3C) and *N. tabacum* (Fig. 3D, 3E) tapetum cells.

Caspase 3-like enzymatic activity was studied by a biochemical assay with the caspase 3 specific substrate, Ac-DEVD-pNA, in the three main stages of the tapetum development described above. Very low caspase 3 activity was detected in “active tapetum” stage (0.12 ± 0.01 μ moles pNA/mg/ml in *Brassica napus* and 0.5 ± 0.01 μ moles pNA/mg/ml in *Nicotiana tabacum*) (Fig. 4), while it increased with development and PCD progression (Fig. 4). The highest levels of caspase 3-activity were detected in the “tapetum at PCD” stage (0.85 ± 0.06 μ moles pNA/mg/ml in *Brassica napus* and 1.28 ± 0.17 μ moles pNA/mg/ml in *Nicotiana tabacum*). With the progression of development, at the “late PCD” stage, the caspase 3 activity levels decreased (0.37 ± 0.02 μ moles pNA/mg/ml in *Brassica napus* and 0.82 ± 0.17 μ moles pNA/mg/ml in *Nicotiana tabacum*) (Fig. 4), although these values were still higher than those found in the “active tapetum” stage. Controls of the enzymatic assay were carried out either by omitting the substrate (Ac-DEVD-pNA) or by using the caspase 3 inhibitor (Ac-DEVD-CHO), both of them resulting in almost null levels of activity in all the stages analyzed of *B. napus* and *N. tabacum* anthers (Fig. 4).

Global DNA methylation levels and 5mdC distribution pattern during tapetum PCD

This study analyzed for the first time the dynamics of DNA methylation as epigenetic mark during a plant PCD process. Quantification of global DNA methylation by high performance capillary electrophoresis (HPCE) and immunofluorescence of 5-methyl-

deoxy-cytidine (5mdC) were performed at the three main stages of the tapetum development already described: “active tapetum”, “tapetum at PCD” and “tapetum at late PCD”. HPCE results showed that global DNA methylation increased during the progression of tapetum PCD (Fig. 5A). In the first stage analyzed, when the tapetum cells were active, the DNA methylation levels were low ($7.76\% \pm 1.76$). Later in development, at vacuolated microspore stage, the tapetum started its degradation (stage of “tapetum at PCD”) and the DNA methylation levels increased significantly ($23.82\% \pm 1.74$). The highest DNA methylation values were obtained in the last developmental stage analyzed, in which the tapetum was “at late PCD” stage ($30.30\% \pm 1.02$). These results indicated that the tapetum highly modified the DNA methylation during the PCD process (Fig. 5A).

Confocal microscopy analysis of the 5mdC immunofluorescence assays revealed the nuclear distribution of methylated DNA in tapetal cells and showed an increase in the intensity of the immunofluorescence signal as well as specific changes in the distribution pattern of 5mdC during the PCD (Fig. 5B-5D). Electron microscopy (EM) immunogold labeling of 5mdC showed the precise ultrastructural distribution of the methylated DNA residues over the nuclear domains (Fig. 6). The changes of 5mdC distribution observed were associated with the reorganization of the chromatin condensation pattern that takes place during the PCD process. In the “active tapetum” stage, 5mdC showed a pattern of distribution similar to the condensed chromatin pattern typical of each plant species. In *N. tabacum* 5mdC showed a punctuate pattern as small spots distributed through the whole nuclear area (Fig. 5B, 5B’) fitting with the condensed chromatin pattern characteristic of tobacco cells (Coronado et al. 2007), whereas in *B. napus*, 5mdC labeling was lower and localized mostly at the periphery of the nucleus (Fig. 6A, 6D), where heterochromatin masses are typically located in this specie (Seguí-Simarro et al. 2011, Solís et al. 2012). With the progression of the PCD process, the nuclei of the tapetum cells acquire apoptotic features like high chromatin condensation and nuclear lobulation; at the same time the 5mdC immunofluorescence signal increased and covered larger nuclear areas (Fig. 5C, 5D). The immunogold labeling results revealed the ultrastructural distribution of 5mdC over heterochromatin masses and an increase on the 5mdC labeling density in the nuclei of the tapetum cells with the progression of PCD (Fig. 6A, 6B). Gold particles appeared specifically distributed over the condensed chromatin regions in the nucleus, while no labeling was observed in the cytoplasm of the tapetum cells at different stages. In the “active tapetum” stage, the scarce gold particles were observed as clusters of a few

particles on the small masses of condensed chromatin (Fig. 6A, 6D). On the contrary, on sections from “tapetum at PCD” stage, a higher 5mdC immunogold labeling was observed on the larger condensed chromatin masses which were decorated by numerous immunogold particles (Fig. 6B, 6E). A few gold particles also appeared isolated in some areas of the interchromatin region, over stained thick fibers, probably corresponding to chromatin threads, being the intensity of labeling very much lower in the interchromatin domain (Fig. 6E). This change of ultrastructural pattern of distribution of 5mdC gold labeling correlated with the increasing chromatin condensation observed during PCD (Fig. 2).

The specificity of the immunofluorescence and the immunogold labeling patterns obtained was demonstrated by the three control assays performed: the elimination of the first antibody, the omitting the DNA denaturation step, and the immunodepletion experiment, all of them completely abolished the labeling (Fig. 6C).

DNA methyltransferase *MET1* expression pattern during tapetum PCD

The expression of the DNA methyl-transferase *MET1* of *Nicotiana tabacum* (*NtMET1*) and *Brassica napus* (*BnMET1*), that codify one of the major enzymes responsible of DNA methylation, was analyzed by RT-PCR analysis and fluorescence *in situ* hybridization (FISH) at the three main stages of the tapetum development already described: “active tapetum”, “tapetum at PCD” and “tapetum at late PCD”.

The RT-PCR results showed similar expression patterns for both *BnMET1* and *NtMET1* genes. *MET1* expression was developmentally up-regulated during tapetum PCD observing the highest expression levels in “tapetum at late PCD” stage (Fig. 7A, 7B). To analyze the spatial expression pattern and the subcellular distribution of the *MET1* transcripts, fluorescent *in situ* hybridization (FISH) studies were carried out followed by confocal microscopy analysis. Results showed similar patterns of distribution for FISH signals in the two species, *Nicotiana tabacum* (Fig. 7C-7H) and *Brassica napus* (data not shown). In the “active tapetum” stage, FISH experiments provided a low hybridization signal in the cytoplasm of the tapetal cells, while the rest of the cells of the anther appeared negative (Fig. 7C, 7F). Later, in “tapetum at PCD” stage, high fluorescent signal was observed in the cytoplasm of tapetal cells corresponding to the presence of abundant

transcripts, whereas the rest of the somatic anther tissues did not show any FISH signal (Fig. 7D, 7G). In “tapetum at late PCD” stage, high fluorescence signal was also observed in the cytoplasm of the tapetum cells (Fig. 7E, 7H). No hybridization signal was observed in control experiments with the sense probe in all stages (inset in Fig. 7E).

DISCUSSION

The main goal of this work was to analyze the possible relationship between epigenetic mechanisms, specifically DNA methylation, and the PCD process of the tapetum. For this purpose, the dynamics of DNA methylation during PCD of tapetal cells was characterized by a multidisciplinary approach in two different species, *Brassica napus* and *Nicotiana tabacum*. The characterization of the main subcellular rearrangements and apoptotic-like features of the tapetum during key developmental stages was performed to monitor the process and to identify the PCD events that accompany the epigenetic changes. The results obtained were similar in both species and constitute new findings which provide new insights about a possible epigenetic regulation of the tapetum PCD process.

There is not a clear consensus on the types of PCD occurring in plants, some works claimed that only necrosis and vacuolated/autophagy-like cell deaths pathways are found in plants (van Doorn 2011, van Doorn et al. 2011), while many others have reported evidences of apoptotic-like PCD (Wang et al. 1996, Balk and Leaver 2001, Watanabe et al. 2002, Vacca et al. 2006, Reape and McCabe 2008, Doyle et al. 2010, Reape and McCabe 2010, Alden et al. 2011, Kacprzyk et al. 2011, Tewari et al. 2012), these works are based on the manifestation of a number of morphological and biochemical markers of apoptosis in different plant systems. In the tapetum, some works have also referred to its degeneration as an apoptotic-like PCD process (Rogers 2006, Parish and Li 2010). The results reported in the present study illustrate, in two different plant species, *B. napus* and *N. tabacum*, that tapetum cells undergo a developmental PCD process characterized by defined cellular events such as release of the cytochrome C, chromatin condensation and nuclear lobulation, and gradual loss of cell shape and integrity, all of them typical features of the apoptotic pathway in animals. The partial release of cytochrome C from the mitochondria into the cytosol has been reported as an early event in apoptotic-like PCD of various plant systems (Vacca et al. 2006) and also in tapetal cells of sunflower (Balk and Leaver 2001); in this species, an immunocytochemical analysis with anti-cytochrome C antibodies has provided both punctate and diffuse cytoplasmic signals at the apoptotic-like PCD initiation (Balk and Leaver 2001), analogous patterns to those found in the present work in tapetum cells of canola and tobacco. We have also found in the advanced PCD stages special structures, similar to the “heterogeneous ectopic RNP-derived structures” (HERDS)

previously described in animal cells as the structural sign of transcriptional arrest and apoptosis (Biggiogera and Pellicciari 2000). RNP segregation leading to the formation of HERDS has been reported in a variety of conditions involving a physiological or experimentally-induced decrease of transcription and apoptosis (Biggiogera and Pellicciari 2000, Biggiogera et al. 2004). The finding of these HERDS structures in plants cells provides a new evidence of similarities between animal and plant PCD pathways.

While in animals caspases act as mediators in the initiation and execution of PCD (Bonneau et al. 2008), no caspase gene homologues have been found in plants. Nevertheless, evidence does exist to suggest that caspase 3-like enzymatic activities induce plant cell death (Lord and Gunawardena 2012) and are involved in different processes of PCD such as for example, self-incompatibility in *Papaver* pollen (Lam 2004, Thomas and Franklin-Tong 2004, Bosch and Franklin-Tong 2007) or stress-induced microspore embryogenesis and embryogenic suspension cultures stress response in barley (Rodríguez-Serrano et al. 2012). Plant proteases other than caspase-like enzymes may be involved in PCD; recent papers have shown that aspartic proteases also play a critical role in tapetum PCD (Parish and Li 2010, Phan et al 2011, Phan et al. 2012, Niu et al 2013), these papers among others demonstrated that several types of proteolytic activities are taken part in tapetum PCD in different species. Our results showed for the first time caspase 3-like activity in the tapetum PCD, specifically in *B. napus* and *N. tabacum*. Efforts to purify and characterize the proteases responsible for the caspase-like activities in plant cells have indicated that serine proteases and a vacuolar processing enzyme, which is a cysteine protease, might potentially account for the caspase-like activities in plant PCD (Coffeen and Wolpert 2004, Hatsugai et al. 2004), as well as the proteasome subunit PBA1 (Hatsugai et al. 2009); also, the participation of proteosomes with different protease activities in the tapetum PCD has been suggested (Parish and Li 2010). The present results suggest that plant proteases might be active during tapetum PCD in *N. tabacum* and *B. napus*, some of them having similar substrate, enzymatic activity and inhibitor properties as the mammalian caspase 3. This result provides new evidence to the existence of specific proteases with similar activity to caspases 3, in the tapetal cells undergoing PCD.

When comparing the progression of PCD with the epigenetic mark dynamics (Fig. 8), our results show, in both plant species studied, that increase in DNA methylation and *MET1* gene expression take place at the developmental stage in which cells show typical

morphological apoptotic-like features of the initiation of the process: reorganization of the nuclear domains architecture (lobulated nuclei, high degree of chromatin condensation, fragmentation of the nucleolus and RNP segregation), activity of caspase 3-like proteases and release of cytochrome C (Fig. 8). Moreover, the increase of the global DNA methylation levels is accompanied by a change of the 5mdC distribution pattern during the tapetum PCD process. At the same time, these epigenetic changes correlate with the up-regulation of *MET1* expression pattern. These facts might be linked to the global changes in chromatin condensation and nuclear organization that accompany the PCD process.

Although the quantification of DNA methylation is important as a global parameter of gene expression (Kouzarides 2007, Valledor et al. 2007) the immunolocalization studies carried out in this work also revealed the dynamics of the 5mdC nuclear distribution pattern during the progression of PCD in relation to the dynamics of chromatin condensation pattern of the tapetum cells, at different developmental stages. The immunolabeling analyses showed not only an increase on the 5mdC labelling with the PCD progression, but also a change in the distribution pattern of 5mdC, starting with small nuclear spots at metabolically active stages and finishing with large nuclear masses corresponding with highly condensed chromatin masses at later stages of the PCD process; this dynamics of the 5mdC distribution pattern correlated with the chromatin condensation process that occurs during PCD (Fig. 8).

DNA methylation plays an essential role in plant development as a mechanism to epigenetically maintain developmental decisions in proliferating and differentiating cells (Valledor et al. 2007, Berdasco et al. 2008, Meijón et al. 2009, Solís et al. 2012, Testillano et al. 2013). In the present work, the changes in the distribution of 5mdC observed in different phases of anther development suggest DNA methylation as an epigenetic mechanism in chromatin remodeling during the tapetum PCD process, and maybe a different role of epigenetic marks in apoptotic cells than in proliferating/differentiating cells. The high accuracy of the confocal microscopy analysis, together with the high resolution provided by the immunogold labeling assay at the EM level, indicated that 5mdC distribution pattern is associated with the condensed chromatin and increases with the tapetum degradation. While in differentiating cells, DNA methylation dynamics regulates the ability to remodel chromatin organization and gene silencing, providing the basis for the plasticity in plant cell fate changes (Costa and Shaw 2007), in the case of

PCD, DNA methylation could be involved not only in transcriptional arrest and gene silencing mechanisms, but also in the profound reorganization of the nuclear architecture and chromatin condensation associated with the PCD process.

The monitoring of the expression of the DNA methyltransferases Nt*MET1* and Bn*MET1* indicate a dynamic pattern that changes with the progression of the PCD process and correlates with the DNA methylation changes (Fig. 8), suggesting the participation of MET1 in the methylation events of tapetum cells during PCD. *MET1* homologues have been characterized in various plants, being expressed in vegetative and reproductive organs (Fujimoto et al. 2006, Solís et al. 2012). The dynamic expression pattern of *MET1* genes during plant development has already been described in other plant systems and species (Yamauchi et al. 2008, Solís et al. 2012). Besides, FISH experiments allowed us the localization of *MET1* transcripts in the cytoplasm of the *B. napus* and *N. tabacum* tapetum cells showing significant differences among each developmental stage: scarce transcripts localization in the cytoplasm of the active tapetum cells and a significant increase in transcripts during initiation and progression of tapetum PCD.

The parallelism between 5mdC immunofluorescence and *MET1*-FISH signals in the tapetum cells during microspore-early pollen development, suggests that the MET1 activity would be responsible, at least in part, of DNA methylation increases during this process, being its activity regulated mainly at transcriptional level. This correlation has also been found in different stages of embryogenesis and pollen development (Solís et al. 2012), suggesting that MET1 has an essential role, not only in the maintenance but also in *de novo* DNA methylation during microspore-early pollen development and embryogenesis. Nevertheless, the high levels of global DNA methylation observed during tapetum PCD might suggest the existence of additional methylating mechanisms apart from MET1 activity.

Conclusions

The findings reported in this work reveal for the first time the existence of epigenetic changes during the tapetum PCD process. The multidisciplinary approach performed here has provided data which indicates a relation between the PCD process and the DNA methylation dynamics and *MET1* DNA methyltransferase expression in tapetal

cells, opening new lines of evidence for the relevance of epigenetic control of PCD. Results show in both *B. napus* and *N. tabacum*, that tapetum PCD progresses with the increase in global DNA methylation and *MET1* expression, epigenetic changes which take place together with the reorganization of the nuclear architecture, high chromatin condensation, activity of caspase 3-like proteases and release of cytochrome C. The relation established in the present work, between the tapetum PCD process and the changes in DNA methylation might indicate that this epigenetic mark could play a new role in the processes of chromatin condensation and reorganization of the nuclear architecture associated with the PCD, as well as in the inactivation and gene silencing mechanisms of the tapetum during PCD. This information gives new insights in the knowledge of the epigenetic regulation of the PCD processes.

MATERIAL AND METHODS

Plant material

Plants were grown under controlled conditions: 15°C day, 16h photoperiod, 10°C night and 60% humidity for *Brassica napus* L. cv. Topas and 25°C with a 16 h light/8 h dark cycle and 80% humidity for *Nicotiana tabacum* L. cv. Petit Habana. Anthers from different bud sizes were collected and processed for different assays. For HPCE, Western blot and RT-PCR studies anthers were rapidly frozen in liquid nitrogen, previously microspores were gently extracted from the anthers. For immunofluorescence and FISH, anthers were fixed and cryoprocessed as described below.

Cryoprocessing for *in situ* localization assays

Anthers at different developmental stages were collected and fixed in 4% paraformaldehyde in PBS, pH 7.3, overnight at 4°C. For immunofluorescence and FISH assays, paraformaldehyde fixed anthers were processed by two main protocols (Solís et al. 2012). A set of samples were dehydrated, embedded in Historesin Plus at 4°C and sectioned at 2 µm thickness using the ultramicrotome (Ultracut E Reichert). Other group of samples was cryoprotected in 2.3M sucrose, embedded in tissue-freezing medium, frozen on dry ice and sectioned in a cryostat at 40 µm thickness (Leica Cm 1800). All resin and cryostat sections were mounted on slides coated with APTES (3-aminopropyltriethoxysilane, Sigma). Resin sections were used for anti-RNA and 5mdC immunofluorescence and cryostat sections were used for cytochrome C immunofluorescence and FISH assays.

For immunogold labeling, fixed samples were dehydrated by PLT (Progressive Lowering of Temperature) method in a Leica AFS system and embedded in Lowicryl K4M resin at -30°C under UV light.

Antibodies

The antibodies used in this study were: mouse monoclonal anti-5mdC (Eurogentec, Cat. no. BI-MECY-0100), mouse monoclonal anti-RNA D44 (Mena et al. 1994) and

mouse monoclonal anti-cytochrome C (BD Biosciences) For the immunodepletion control experiments the following immunogen was used: 5mdC (Sigma-Aldrich).

Immunofluorescence

Frozen slides carrying cryostat sections were permeabilized by dehydration-rehydration in methanol series followed by treatment with 2% cellulase (Ozonuka R-10) for 1h at room temperature, washed in PBS and incubated in 5% bovine serum albumin (BSA) in PBS for 10 min. In contrast, semithin resin sections were directly washed with PBS and blocked with BSA. Then, both types of sections were treated equally for immunofluorescence as previously described (Testillano et al. 2005, Testillano and Risueño 2009). Only in the case of 5mdC localization, sections were first denaturated with 2N HCl for 45 min and washed in PBS before the primary antibody incubation (Testillano et al. 2013). Primary antibodies were incubated at the following dilutions: anti-5mdC diluted 1/50; anti-RNA, undiluted and anti-cytochrome C diluted 1/50 in 1% BSA in PBS. The signal was revealed with the appropriate Alexa Fluor 488-labelled anti-mouse antibodies (Molecular Probes) diluted 1/25 in PBS for 45 min in the dark. Finally, the slides were counterstained with 1mg/ml DAPI (4', 6-diamidino-2-phenylindole; Fluka) solution for 10 min. Immunodepletion negative controls were performed replacing the primary antibody by the preblocked antibody with its specific immunogen, for anti-5mdC, 5mdC was used as previously described (Testillano et al. 2013).

Immunofluorescence preparations were analyzed using a confocal microscope (Leica TCS-SP5). Z-optical sections were captured at intervals of 0.5 μ m and projections of several optical sections (4 and 10 sections for resin and cryostate sections respectively) were obtained for each preparation. For making accurate and reliable comparison among fluorescence signals, the same settings for laser excitation and image acquisition were kept in the confocal microscope and used for analysis of all samples of the same antibody.

Protein extraction, SDS-PAGE and Western blotting

Total proteins were extracted from 100 mg of anthers (fresh weight) as described (Coronado et al. 2007) and quantified using the Bradford assay (Bio-Rad), with ovalbumin as standard. Equal amounts of proteins for each sample and standards were separated by

electrophoresis (110 V) in 15% acrylamide SDS gels (Mini-PROTEAN II Multi-Casting Chamber; BIO-RAD) for cytochrome C detection, and then transferred to Immobilon membranes (Millipore Corp., Bedford, MA) by electroblotting (350 mA for 2 h). For immunodetection, strips were blocked in a 1.5% dilution of powdered skimmed milk in 5x TBS buffer (20 mM Tris-HCl, pH 7.8 and 0.18M NaCl) at 4°C overnight. Then, membranes were incubated for 1 h with anti-cytochrome C antibody diluted 1/300 in the blocking solution. After three washes (10 min each) with 1x TBS, membranes were incubated for 2 h with the corresponding secondary antibodies anti-mouse IgG conjugated with HRP diluted 1/2500. After three more washes, proteins were revealed by ECL substrates and visualized with a luminescent image analyzer. Strips were stained, prior to the immunodetection with Ponceau Red for total protein detection.

Caspase 3 enzymatic activity assay

Caspase 3-like activity was analyzed in anthers from different bud sizes, as previously described (Rodríguez-Serrano et al. 2012) using the Caspase 3 Assay Kit, Colorimetric (CASP3C, Sigma Aldrich), based on the hydrolysis of the peptide substrate acetyl-Asp-Glu-Val-Asp p-nitroanilide (Ac-DEVD-pNA) by caspase 3, which results in the release of the p-nitroaniline (pNA) moiety. The concentration of the pNA released from the substrate is calculated from the interpolation of the absorbance values at 405 nm in the calibration curve prepared with defined pNA solutions. Controls were performed in duplicate samples which were incubated in parallel either in the absence of the substrate or in the presence of a 20 µM caspase 3 inhibitor, Ac-DEVD-CHO. All assays were performed on three independent samples, measured in duplicate and P-values were calculated using the Student-*t* test.

Quantification of global DNA methylation by High Performance Capillary Electrophoresis (HPCE)

Genomic DNA was extracted from 100 mg of anthers (fresh weight) using a plant genomic DNA extraction kit (DNeasy Plant Mini, Qiagen) according to the manufacturer's instructions and adding 10 µl RNase A (Qiagen). The concentration and the hydrolysis of the DNA samples was performed as described (Solís et al. 2012, Testillano et al. 2013).

Hydrolyzed solutions were centrifuged for 20 min at 15,000g. Samples were analyzed according to (Fraga et al. 2002) with the modifications of (Hasbún et al. 2008) by HPCE.

Three biological and two analytical replicates per sample were taken. Quantification of the relative methylation of each DNA sample was performed as the percentage of 5mdC peak of total deoxycytidines (dC+5mdC) peaks. P-values were calculated using Student-*t* test.

Immunogold labeling for electron microscopy

Lowicryl ultrathin sections were obtained in an ultramicrotome (Ultracut E Reichert) and collected on 200-mesh nickel grids with a carbon-coated Formvar supporting film. Ultrathin sections were floated on drops of distilled water, denaturated with 2N HCl for 45 min and washed in PBS before the incubation in 5% BSA. For immunogold labeling, they were incubated with anti-5mdC antibody (diluted 1:50) for 1 h at room temperature. After washing with PBS, the sections were incubated with anti-mouse secondary antibody conjugated to 10 nm gold particles (BioCell, Cardiff, Wales, U.K.) diluted 1/25 in PBS for 45 min. Then, the grids were washed in PBS, rinsed in distilled water and air-dried. Finally, the grids were counterstained with 5% uranyl acetate and 1% lead citrate, and observed with a JEOL 1010 microscope operating at 80 kV.

For ultrastructural analysis, some sections without immunogold labelling were stained with EDTA regressive staining, preferential for RNPs (Bernhard 1969).

RT-PCR Analysis

Total RNA was isolated from anthers of different bud sizes, using the RNeasy Plant Minikit (Qiagen) according to the manufacturer's instructions. One microgram of total RNA was used for the RT reaction using the Superscript TM II reverse transcriptase enzyme (Invitrogen). For *NtMET1* expression analysis, the oligonucleotides used were 5' TGCAGCAATGGATGAGAACG 3' and 3' ACAGTAAGCGAACGGAATGG 5' (AB280788.1) designed from the sequence of one of the MET1 DNA methyltransferases characterized in *Nicotiana tabacum* (Kim et al. 2007). For *BnMET1* analysis, the oligonucleotides were: 5' GGCAGACGTTCCAACCTACT 3' and

3'AAGGTGCACCGTATTGAGTA 5' from the sequence of the BrMET1a gene (AB251937.1), one of the MET1 DNA methyltransferases characterized in *Brassica rapa* (Fujimoto et al. 2006). For Actin II analysis (used as control), the oligonucleotides were: 5'CTCGGCACACTGGTGTTCATG 3' and 3'CGTTTGGATCTCGCTGGTTCG 5'. cDNAs were amplified by PCR using the Hot Master Taq polymerase (Eppendorf). PCR products were detected on 1% agarose gels stained with ethidium bromide. Band intensity was expressed as relative absorbance units. Each cDNA band density was first normalized by dividing it by the density of the actin II band in the same lane.

Fluorescence *in situ* hybridization (FISH)

For probe preparation, cDNA was obtained as described before and used for PCR amplification with the *NtMET1* primers mentioned above. The amplified fragments were isolated from an agarose gel and cloned using a pGEMT-Easy cloning system (Promega). dig-RNA-MET1 probes were generated by *in vitro* transcription using the DIG-RNA-labeling kit (Roche).

Frozen slides carrying cryostat sections were permeabilized by dehydration-rehydration in methanol series followed by treatment with 2% cellulase (Ozonuka R-10) for 1h, washed and dried. RNA/RNA *in situ* hybridization was performed as described (Solís et al. 2012) using dig-RNA-MET1 probes diluted 1/50 in hybridization buffer at 50°C, overnight. Post-hybridization washes were performed in 4xSSC, 2xSSC and 0,1xSSC. Hybridization signal was detected by immunofluorescence with anti-digoxigenin antibodies as described (Solís et al. 2012). After washing in PBS, sections were counterstained with DAPI, mounted in Mowiol, and observed in a confocal microscope (Leica TCS-SP5). Controls were performed with the sense probe.

FUNDING

This work was supported by projects of Spanish Ministry of Economy and Competitiveness, MINECO (BFU2011-23752), and Spanish National Research Council, CSIC (201020E038).

ACKNOWLEDGEMENTS

Thanks are due to Ms. Alicia Rodríguez-Huete for her skillful technical assistance. NC and JCE were recipients of grants of the Spanish Ministry of Science and Innovation, MICINN, for Stays of Foreign Postdoctoral Researchers and for Sabaticcal Stays respectively in Spanish Research Centres. MRS was recipient of a postdoctoral Juan-de-la-Cierva grant (JCI-2007-123-1177) of the Spanish MICINN.

REFERENCES

- Alden, K. P., Dhondt-Cordelier, S., McDonald, K. L., Reape, T. J., Ng, C. K., McCabe, P. F. and Leaver, C. J.** 2011. Sphingolipid long chain base phosphates can regulate apoptotic-like programmed cell death in plants. *Biochem Biophys Res Commun*, 410, 574-580.
- Balk, J. and Leaver, C. J.** 2001. The PET1-CMS mitochondrial mutation in sunflower is associated with premature programmed cell death and cytochrome c release. *Plant Cell*, 13, 1803-1818.
- Berdasco, M., Alcazar, R., Victoria García-Ortiz, M., Ballestar, E., Fernández, A. F., Roldán-Arjona, T., Tiburcio, A. F., Altabella, T., Buisine, N., Quesneville, H., Baudry, A., Lepiniec, L., Alaminos, M., Rodríguez, R., Lloyd, A., Colot, V., Bender, J., Jesús Cañal, M., Esteller, M. and Fraga, M. F.** 2008. Promoter DNA Hypermethylation and Gene Repression in Undifferentiated *Arabidopsis* Cells. *PLoS One*, 3, e3306.
- Bernhard, W.** 1969. A new staining procedure for electron microscopical cytology. *J Ultrastruct Res*, 27, 250-265.
- Biggiogera, M., Bottone, M. G., Scovassi, A. I., Soldani, C., Vecchio, L. and Pellicciari, C.** 2004. Rearrangement of nuclear ribonucleoprotein (RNP)-containing structures during apoptosis and transcriptional arrest. *Biol Cell*, 96, 603-615.
- Biggiogera, M. and Pellicciari, C.** 2000. Heterogeneous ectopic RNP-derived structures (HERDS) are markers of transcriptional arrest. *Faseb Journal*, 14, 828-834.
- Bonneau, L., Ge, Y., Drury, G. E. and Gallois, P.** 2008. What happened to plant caspases? *Journal of Experimental Botany*, 59, 491-499.
- Bosch, M. and Franklin-Tong, V. E.** 2007. Temporal and spatial activation of caspase-like enzymes induced by self-incompatibility in *Papaver* pollen. *Proc Natl Acad Sci U S A*, 104, 18327-18332.
- Cedar, H. and Bergman, Y.** 2012. Programming of DNA methylation patterns. *Ann Rev Biochem*, 81, 97-117.
- Coll, N. S., Eppe, P. and Dangl, J. L.** 2011. Programmed cell death in the plant immune system. *Cell Death Differ*, 18, 1247-1256.
- Collazo, C. M., Sher, A., Meierovics, A. I. and Elkins, K. L.** 2006. Myeloid differentiation factor-88 (MyD88) is essential for control of primary *in vivo Francisella tularensis* LVS infection, but not for control of intra-macrophage bacterial replication. *Microbes and Infection*, 8, 779-790.
- Coronado, M. J., Testillano, P. S., Wilson, C., Vicente, O., Heberle-Bors, E. and Risueño, M. C.** 2007. *In situ* molecular identification of the Ntf4 MAPK expression sites in maturing and germinating pollen. *Biol Cell*, 99, 209-221.

- Costa, S. and Shaw, P.** 2007. 'Open minded' cells: how cells can change fate. *Trends Cell Biol*, 17, 101-106.
- Doyle, S. M., Diamond, M. and McCabe, P. F.** 2010. Chloroplast and reactive oxygen species involvement in apoptotic-like programmed cell death in *Arabidopsis* suspension cultures. *J Exp Bot*, 61, 473-482.
- Feng, X. and Dickinson, H. G.** 2010. Tapetal cell fate, lineage and proliferation in the *Arabidopsis* anther. *Development*, 137, 2409-2416.
- Fraga, M. F., Uriol, E., Diego, L. B., Berdasco, M., Esteller, M., Cañal, M. J. and Rodríguez, R.** 2002. High-performance capillary electrophoretic method for the quantification of 5-methyl 2'-deoxycytidine in genomic DNA: Application to plant, animal and human cancer tissues. *Electrophoresis*, 23, 1677-1681.
- Fujimoto, R., Sasaki, T. and Nishio, T.** 2006. Characterization of DNA methyltransferase genes in *Brassica rapa*. *Genes Genet Systems*, 81, 235-242.
- Fullgrabe, J., Hajji, N. and Joseph, B.** 2010. Cracking the death code: apoptosis-related histone modifications. *Cell Death Differ*, 17, 1238-1243.
- Gehring, M. and Henikoff, S.** 2007. DNA methylation dynamics in plant genomes. *Biochimica Et Biophysica Acta-Gene Structure and Expression*, 1769, 276-286.
- Goldberg, R. B., Beals, T. P. and Sanders, P. M.** 1993. Anther development: basic principles and practical applications. *Plant Cell*, 5, 1217-1229.
- Grant-Downton, R. T. and Dickinson, H. G.** 2005. Epigenetics and its implications for plant biology. 1. The epigenetic network in plants. *Ann Bot*, 96, 1143-1164.
- Hasbún, R., Villedor, L., Rodríguez, J. L., Santamaría, E., Ríos, D., Sánchez, M., Cañal, M. J. and Rodríguez, R.** 2008. HPCE quantification of 5-methyl-2 '-deoxycytidine in genomic DNA: Methodological optimization for chestnut and other woody species. *Plant Physiol Biochem*, 46, 815-822.
- Hatsugai, N., Kuroyanagi, M., Yamada, K., Meshi, T., Tsuda, S., Kondo, M., Nishimura, M. and Hara-Nishimura, I.** 2004. A plant vacuolar protease, VPE, mediates virus-induced hypersensitive cell death. *Science*, 305, 855-858.
- Hatsugai, N., Iwasaki, S., Tamura, K., Kondo, M., Fuji, K., Ogasawara, K., Nishimura, M., Hara-Nishimura I.** 2009. A novel membrane fusion-mediated plant immunity against bacterial pathogens. *Genes Dev*, 23, 2496-2506.
- Kacprzyk, J., Daly, C. T. and McCabe, P. F.** 2011. The Botanical Dance of Death: Programmed Cell Death in Plants. *Adv Bot Res*, 60, 169-261.
- Kim, H. J., Yano, A., Wada, Y. and Sano, H.** 2007. Properties of a tobacco DNA methyltransferase, *NtMET1* and its involvement in chromatin movement during cell division. *Ann Bot*, 99, 845-856.
- Kouzarides, T.** 2007. Chromatin modifications and their function. *Cell*, 128, 693-705.

- Lam, E.** 2004. Controlled cell death, plant survival and development. *Nature Rev Mol Cell Biol*, 5, 305-315.
- Li, N., Zhang, D. S., Liu, H. S., Yin, C. S., Li, X. X., Liang, W. Q., Yuan, Z., Xu, B., Chu, H. W., Wang, J., Wen, T. Q., Huang, H., Luo, D., Ma, H. and Zhang, D. B.** 2006. The rice tapetum degeneration retardation gene is required for tapetum degradation and anther development. *Plant Cell*, 18, 2999-3014.
- Lord, C. E. and Gunawardena, A. H.** 2012. The lace plant: a novel model system to study plant proteases during developmental programmed cell death *in vivo*. *Physiologia Plantarum*, 145, 114-120.
- Meijón, M., Valledor, L., Santamaría, E., Testillano, P. S., Risueño, M. C., Rodríguez, R., Feito, I. and Cañal, M. J.** 2009. Epigenetic characterization of the vegetative and floral stages of azalea buds: Dynamics of DNA methylation and histone H4 acetylation. *J Plant Physiol*, 166, 1624-1636.
- Mena, C. G., Testillano, P. S., González-Melendi, P., Gorab, E. and Risueño, M. C.** 1994. Immunoelectron microscopy of RNA combined with nucleic-acid cytochemistry in plant nucleoli. *Exp Cell Res*, 212, 393-408.
- Niu, N., Liang, W., Yang, X., Jin W., Wilson, Z.A., Hu, J., Zhang, D.** 2013. EAT1 promotes tapetal cell death by regulating aspartic proteases during male reproductive development in rice. *Nature Commun*, 4, 1445. doi: 10.1038/ncomms2396.
- Papini, A., Mosti, S. and Brighigna, L.** 1999. Programmed-cell death events during tapetum development of angiosperms. *Protoplasma*, 207, 213-221.
- Parish, R. W. and Li, S. F.** 2010. Death of a tapetum: A programme of developmental altruism. *Plant Sci*, 178, 73-89.
- Phan, H.A., Li, S.F., Parish, R.W.** 2012. MYB80, a regulator of tapetal and pollen development, is functionally conserved in crops. *Plant Mol Biol*, 78, 171-183.
- Phan, H.A., Iacuone, S., Li, S.F., Parish, R.W.** 2011. The MYB80 transcription factor is required for pollen development and the regulation of tapetal programmed cell death in *Arabidopsis thaliana*. *Plant Cell*, 23, 2209-2224.
- Reape, T. J. and McCabe, P. F.** 2008. Apoptotic-like programmed cell death in plants. *New Phytol*, 180, 13-26.
- Reape, T. J. and McCabe, P. F.** 2010. Apoptotic-like regulation of programmed cell death in plants. *Apoptosis*, 15, 249-256.
- Risueño, M. C., Giménez-Martín, G., López-Saez, J. F., and Rodríguez-García, M. I.** 1969. Origin and development of sporopollenin bodies. *Protoplasma*, 67, 361.
- Rodríguez-Serrano, M., Bárány, I., Prem, D., Coronado, M. J., Risueño, M. C. and Testillano, P. S.** 2012. NO, ROS, and cell death associated with caspase-like activity increase in stress-induced microspore embryogenesis of barley. *J Exp Bot*, 63, 2007-2024.

- Rogers, H. J.** 2006. Programmed cell death in floral organs: How and why do flowers die? *Annals of Botany*, 97, 309-315.
- Seguí-Simarro, J. M., Corral-Martínez, P., Corredor, E., Raska, I., Testillano, P. S. and Risueño, M. C.** 2011. A change of developmental program induces the remodeling of the interchromatin domain during microspore embryogenesis in *Brassica napus* L. *J Plant Physiol*, 168, 746-757.
- Solís, M. T., Rodríguez-Serrano, M., Meijón, M., Cañal, M. J., Cifuentes, A., Risueño, M. C. and Testillano, P. S.** 2012. DNA methylation dynamics and *MET1a*-like gene expression changes during stress-induced pollen reprogramming to embryogenesis. *J Exp Botany*, 63, 6431-6444.
- Tessadori, F., van Driel, R. and Fransz, P.** 2004. Cytogenetics as a tool to study gene regulation. *Trends Plant Sci*, 9, 147-153.
- Testillano, P. and Risueño, M.** 2009. Tracking gene and protein expression during microspore embryogenesis by confocal laser scanning microscopy. In *Advances in Haploid Production in Higher Plants*, 8. Edited by Touraev, A. et al. Springer-Verlag, Heidelberg. pp. 339-347.
- Testillano, P. S., González-Melendi, P., Coronado, M. J., Seguí-Simarro, J. M., Moreno-Risueño, M. A. and Risueño, M. C.** 2005. Differentiating plant cells switched to proliferation remodel the functional organization of nuclear domains. *Cytogenet Genome Res*, 109, 166-174.
- Testillano, P. S., González-Melendi, P., Fadón, B., Sánchez-Pina, A., Olmedilla, A. and Risueño, M. C.** 1993. Immunolocalization of nuclear antigens and ultrastructural cytochemistry on tapetal cells of *Scilla peruviana* and *Capsicum annuum*. *Plant System Evol*, Suppl.7, 49-58.
- Testillano, P. S., Solís, M. T. and Risueño, M. C.** 2013. The 5-methyl-deoxy-cytidine localization to reveal in situ the dynamics of DNA methylation chromatin pattern in a variety of plant organ and tissue cells during development. *Physiologia Plantarum*, 149, 104-114.
- Tewari, R. K., Watanabe, D. and Watanabe, M.** 2012. Chloroplastic NADPH oxidase-like activity-mediated perpetual hydrogen peroxide generation in the chloroplast induces apoptotic-like death of *Brassica napus* leaf protoplasts. *Planta*, 235, 99-110.
- Thomas, S. G. and Franklin-Tong, V. E.** 2004. Self-incompatibility triggers programmed cell death in Papaver pollen. *Nature*, 429, 305-309.
- Vacca, R. A., Valenti, D., Bobba, A., Merafina, R. S., Passarella, S. and Marra, E.** 2006. Cytochrome c is released in a reactive oxygen species-dependent manner and is degraded via caspase-like proteases in tobacco Bright-Yellow 2 cells en route to heat shock-induced cell death. *Plant Physiol*, 141, 208-219.
- Vaillant, I. and Paszkowski, J.** 2007. Role of histone and DNA methylation in gene regulation. *Current Opinion Plant Biol*, 10, 528-533.

- Valledor, L., Hasbún, R., Meijón, M., Rodríguez, J. L., Santamaría, E., Viejo, M., Berdasco, M., Feito, I., Fraga, M. F., Cañal, M. J. and Rodríguez, R.** 2007. Involvement of DNA methylation in tree development and micropropagation. *Plant Cell Tiss Organ Cult*, 91, 75-86.
- van Doorn, W. G.** 2011. Classes of programmed cell death in plants, compared to those in animals. *J Exp Bot*, 62, 4749-4761.
- van Doorn, W. G., Beers, E. P., Dangl, J. L., Franklin-Tong, V. E., Gallois, P., Hara-Nishimura, I., Jones, A. M., Kawai-Yamada, M., Lam, E., Mundy, J., Mur, L. A., Petersen, M., Smertenko, A., Taliansky, M., Van Breusegem, F., Wolpert, T., Woltering, E., Zhivotovsky, B. and Bozhkov, P. V.** 2011. Morphological classification of plant cell deaths. *Cell Death Differ*, 18, 1241-1246.
- Vardar, F. and Unal, M.** 2012. Ultrastructural aspects and programmed cell death in the tapetal cells of *Lathyrus undulatus* Boiss. *Acta Biol Hung*, 63, 52-66.
- Wang, C. L., Xu, G. H., Jiang, X. T., Chen, G., Wu, J., Wu, H. Q. and Zhang, S. L.** 2009. S-RNase triggers mitochondrial alteration and DNA degradation in the incompatible pollen tube of *Pyrus pyrifolia* in vitro. *Plant J*, 57, 220-229.
- Wang, H., Li, J., Bostock, R. M. and Gilchrist, D. G.** 1996. Apoptosis: A functional paradigm for programmed plant cell death induced by a host-selective phytotoxin and invoked during development. *Plant Cell*, 8, 375-391.
- Watanabe, M., Setoguchi, D., Uehara, K., Ohtsuka, W. and Watanabe, Y.** 2002. Apoptotic-like cell death of *Brassica napus* leaf protoplasts. *New Phytologist*, 156:417-426.
- Wu, H. M. and Cheung, A. Y.** 2000. Programmed cell death in plant reproduction. *Plant Mol Biol*, 44, 267-281.
- Yamauchi, T., Moritoh, S., Johzuka-Hisatomi, Y., Ono, A., Terada, R., Nakamura, I. and Iida, S.** 2008. Alternative splicing of the rice OsMET1 genes encoding maintenance DNA methyltransferase. *J Plant Phys*, 165, 1774-1782.

FIGURE LEGENDS

Figure 1: Main stages of tapetum development and PCD. A, C, E: Toluidine Blue staining of *Brassica napus* anthers semithin sections. B, D, F: Merged images of total RNA immunofluorescence (green) and DAPI staining of nuclei (blue). A, B: Active tapetum stage. C, D: Tapetum at PCD stage. E, F: Tapetum at late PCD stage. Arrows in A, C and E point to the tapetal nuclei during different developmental stages. AW: anther wall; Tap: tapetum cells; PS: Pollen sac; Mic: Microsporocytes, VM: Vacuolated microspore; YP: Young pollen. Bars: 20µm.

Fig. 2: Ultrastructural changes during tapetum PCD. Electron microscopy images of *Brassica napus* anthers. A, B: Active tapetum stage. C, D: Tapetum at PCD stage. E, F: Tapetum at late PCD stage. A, C, E: Panoramic views of tapetal cells at each stage. B, D: Higher magnification of the tapetum nuclei of each stage. F: Detail showing HERDS-like structures (arrowheads) at late PCD. Arrows in A and B point to the large central nucleolus of the tapetal cell in active stage. Arrow in C points to a nuclear invagination in the tapetal cell at PCD. Arrows in D point to the fragmented nucleolus of cells at PCD. AW: anther wall; Tap: tapetum; PS: pollen sac; Cyt: cytoplasm; N: nuclei. Bars: A, C, E: 2µm; B, D: 1µm; F: 0.2µm.

Figure 3: Immunoblotting and immunolocalization of cytochrome C during tapetum PCD. A: Immunoblotting of cytochrome C in active tapetum and tapetum at PCD of *Brassica napus* anthers revealing a band corresponding to 12 kDa, the expected MW of cytochrome C, in both developmental stages. B, C, D, E: Cytochrome C immunofluorescence. B', C', D', E': DAPI staining of the same structures than in B-E. B, B', C, C': *N. tabacum* cells at the developmental stages of “active tapetum” (B, B') and “tapetum at PCD” (C, C'). D, D', E, E': *B. napus* cells at the developmental stages of “active tapetum” (D, D') and “tapetum at PCD” (E, E'). Immunofluorescence signal in active tapetum cells is punctuate corresponding to mitochondrial localization, whereas signal is punctuate and difusse in cytoplasm in cells at PCD, indicating the partial release of the cytochrome C to the cytoplasm at PCD. Bars in B, B', C, C': 75 µm, in D, D', E, E': 50 µm.

Figure 4: Caspase 3-like enzymatic activity during tapetum PCD. Histogram representing the caspase 3-like activity in the three stages of the tapetum development of *Nicotiana tabacum* (white columns) and *Brassica napus* (dark grey columns) anthers. Negative controls avoiding the substrate (light grey columns) and with the caspase 3 inhibitor (black columns) in *N. tabacum* and *B. napus* anthers respectively. All columns show significant differences at $P < 0.05$ according to Student-*t* test, except all negative controls which are not significantly different among them.

Figure 5: Quantification of DNA methylation by HPCE and 5mdC immunolocalization during tapetum PCD. A: Histogram representing 5mdC percentage in different developmental stages of *Nicotiana tabacum* anthers. Letters indicate significant differences at $P < 0.001$ according to Student-*t* test. B, C, D are the same structures as in B', C', D'. B-D: 5mdC immunofluorescence signal. B', C', D': DAPI staining of nuclei. B, B': Active tapetum stage. C, C': Tapetum at PCD stage. D, D': Tapetum at late PCD stage. Bars: 20 μm .

Figure 6: 5mdC immunogold labeling during tapetum PCD. Electron microscopy images of *Brassica napus* anthers. A, D: Active tapetum stage. B, E: Tapetum at PCD stage. A, B: Panoramic views of tapetal cells at each stage. D, E: High magnification of the nuclear regions squared in (A) and (B) showing the 5mdC immunogold labeling over small peripheral chromatin patches in active tapetum cells (D), and decorating larger condensed chromatin masses in tapetum cells at PCD (E). C: Negative control of the 5mdC immunogold labeling by immunodepletion of the antibody, high magnification of an active tapetum cell, no gold particles are observed. Cyt: cytoplasm; Chr: chromatin; Bars: A, B: 1 μm ; C, D, E: 0.2 μm .

Figure 7: NtMET1 and BnMET1 DNA methyltransferases expression during tapetum PCD. A, B: Semiquantitative RT-PCR histograms showing relative *MET1* expression levels in different developmental stages of anthers of *Nicotiana tabacum* (A) and *Brassica napus* (B). Representative agarose electrophoresis gels of the amplification products of *MET1* and Actin, as housekeeping gene. Columns represent means of mRNA expression of *MET1* \pm SE in arbitrary units (a.u.). C-H: Merged images of Nt*MET1*-FISH (fluorescent *in situ* hybridization) signals (green) and DAPI staining of nuclei (blue) in tobacco anthers. C, F: Active tapetum stage. D, G: Tapetum at PCD stage. E, H: Tapetum at late PCD stage.

C, D, E: Panoramic views of each stage. F, G, H: Higher magnification images of tapetum cells of each stage. Inset in E: Control of FISH experiment performed with the sense probe. AW: anther wall; Tap: tapetum; PS: pollen sac. Bars in C, D, E: 50µm; in F, G, H and inset: 25 µm.

Figure 8: Summary of results on levels of DNA methylation, *MET1* expression and apoptotic-like features during different stages of tapetum PCD; the corresponding pollen developmental stages are also indicated. (+) low levels; (++) mid-high levels; (+++) highest levels.

Figure 1

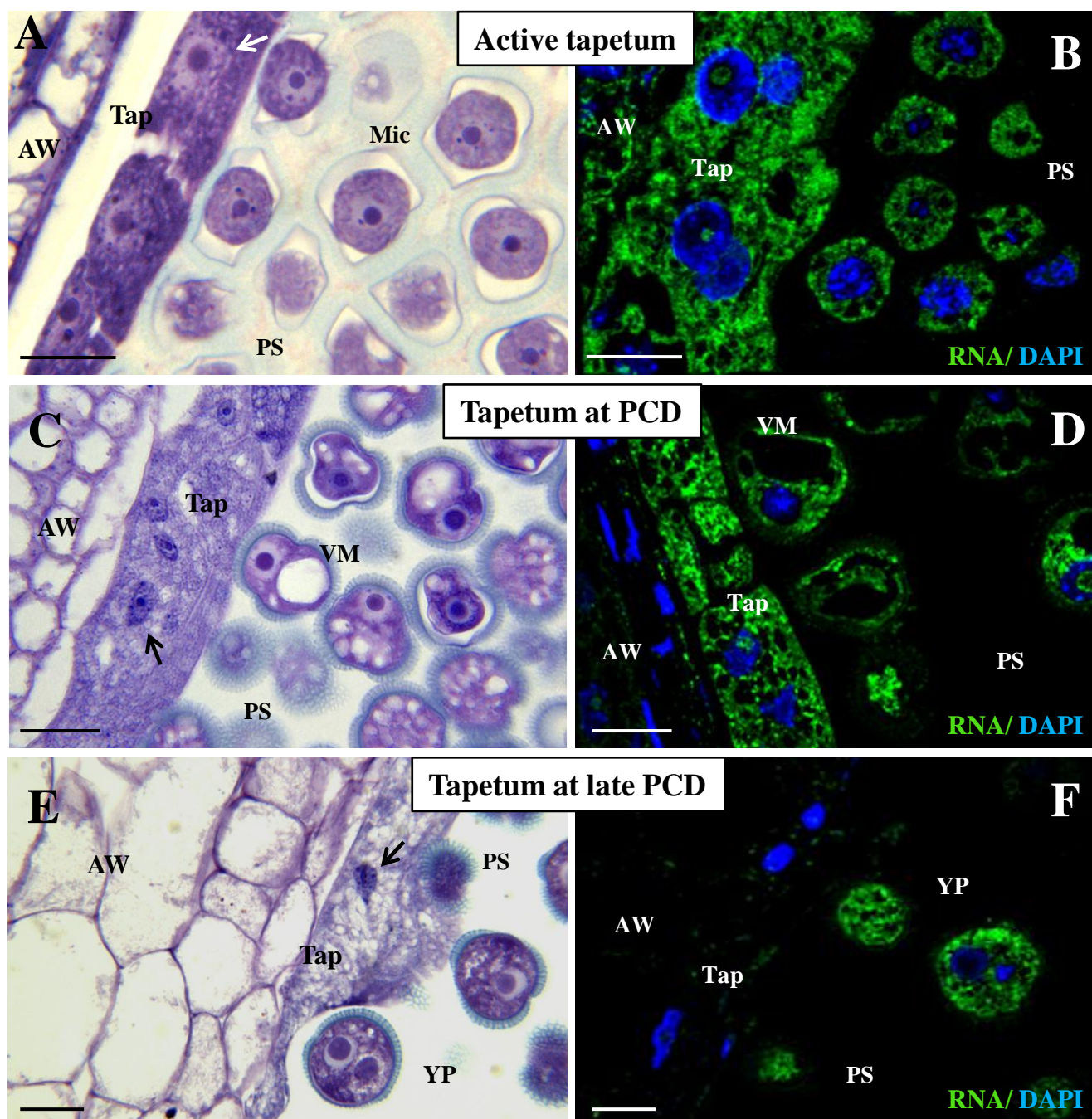


Figure 2

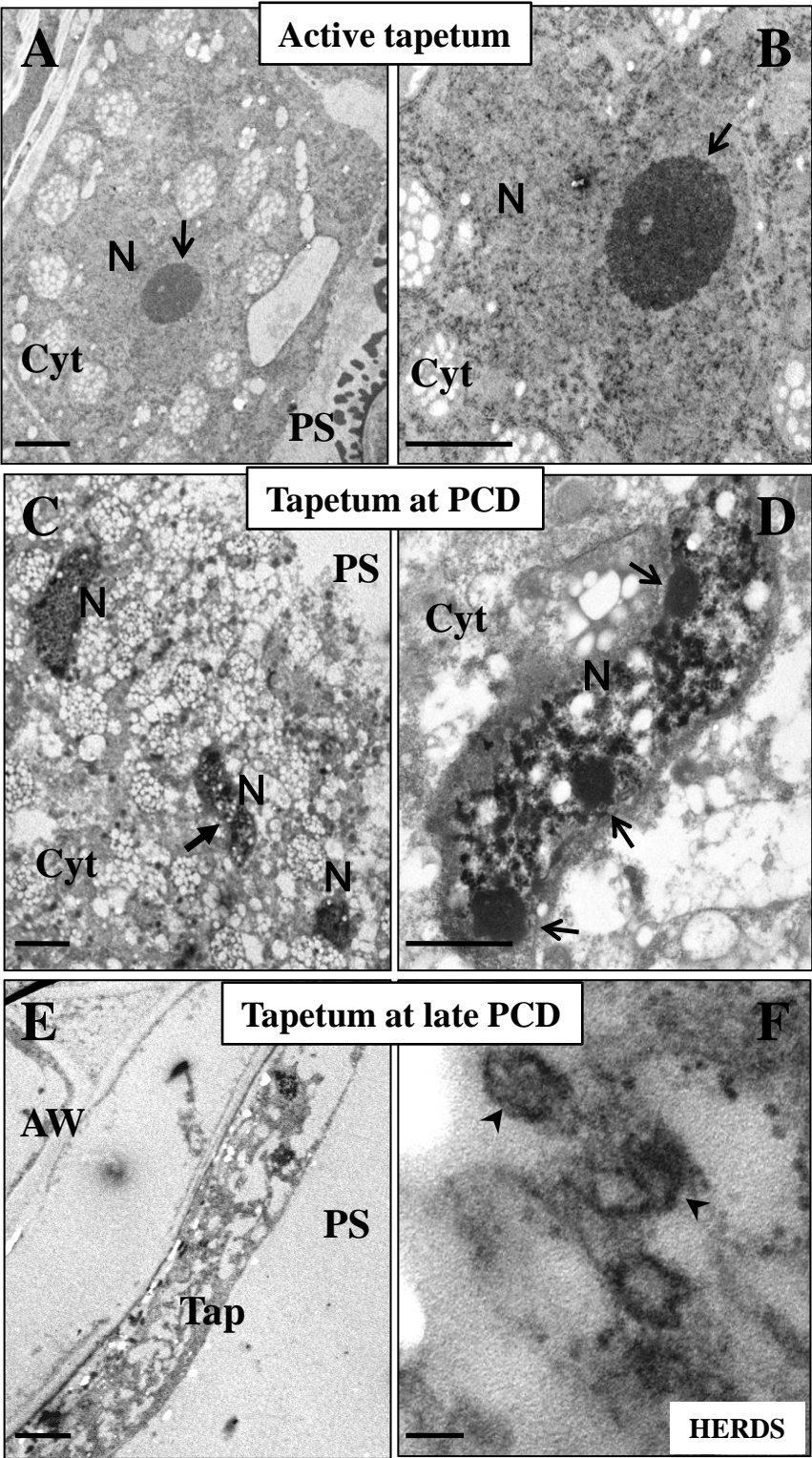


Figure 3

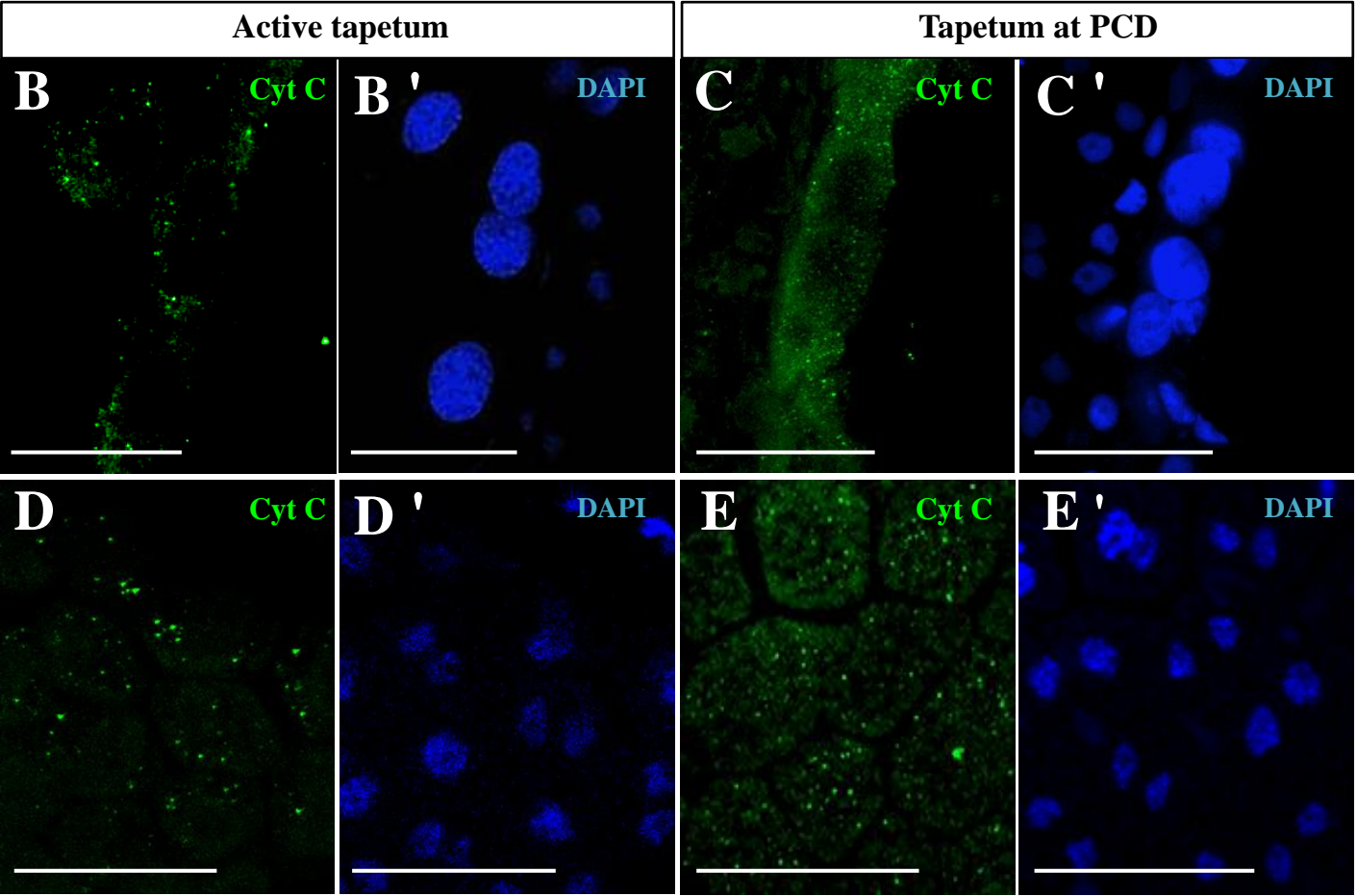
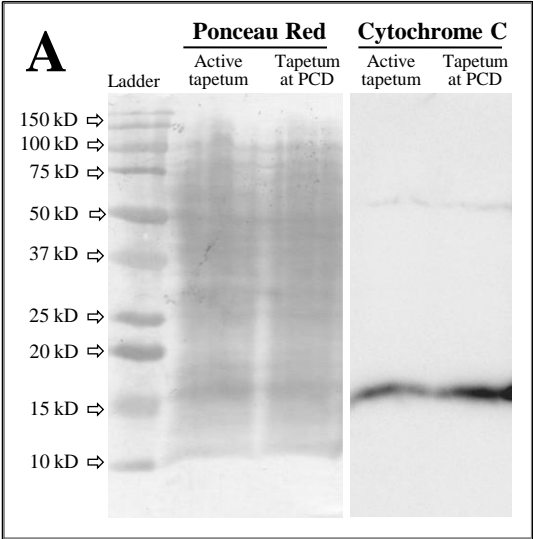


Figure 4

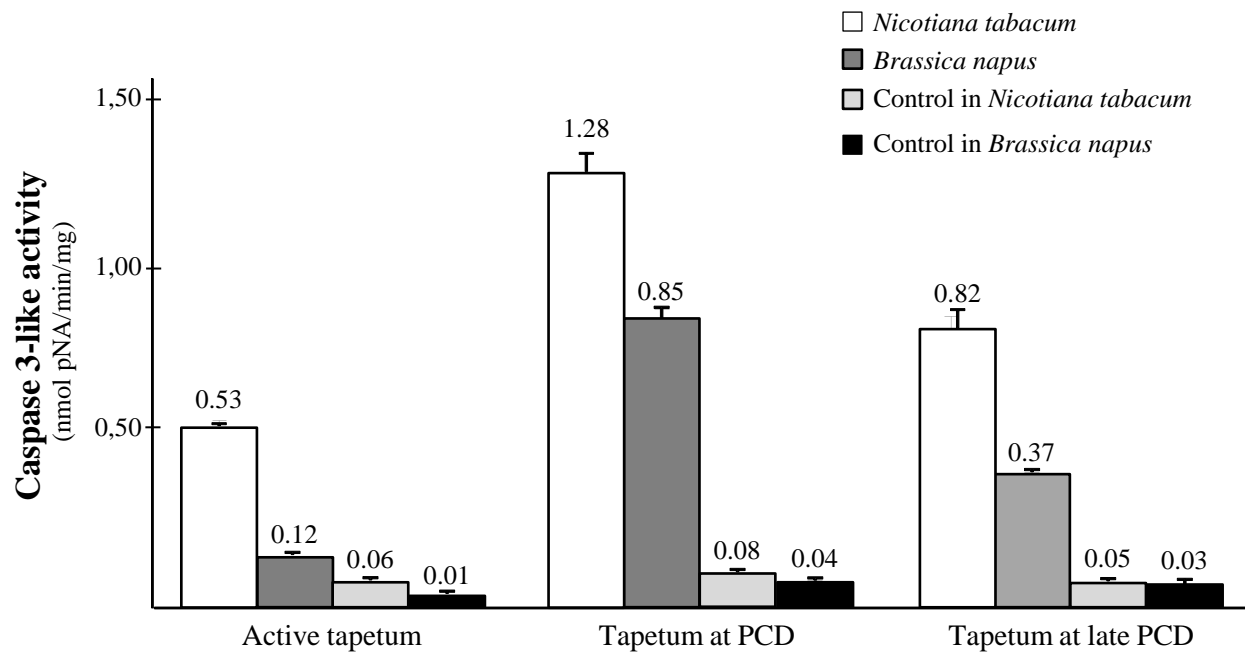


Figure 5

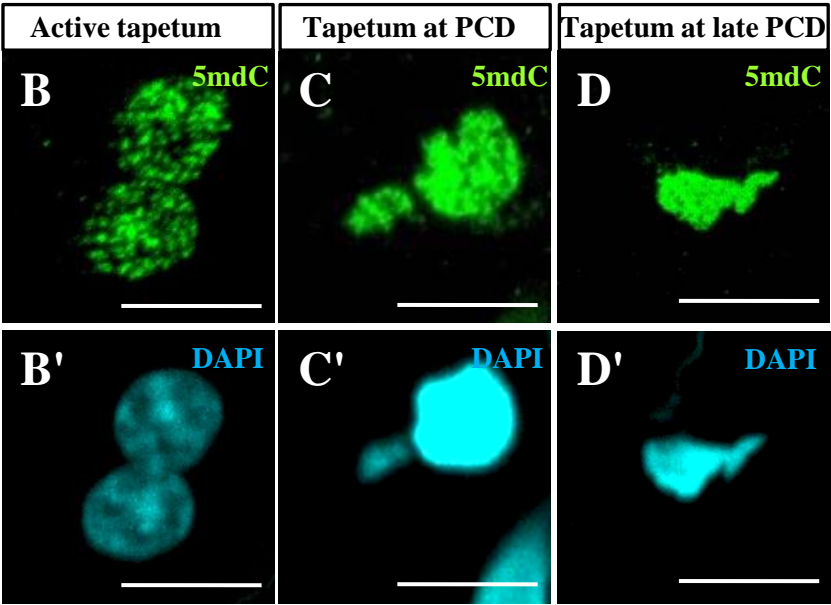
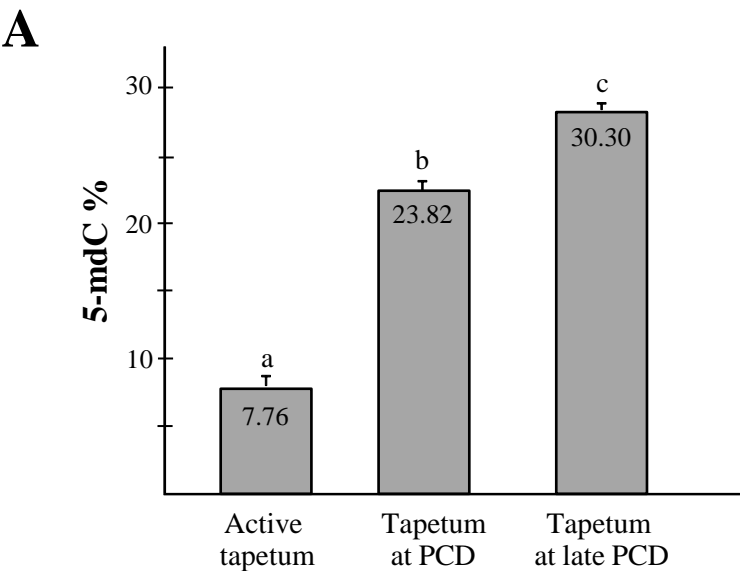


Figure 6

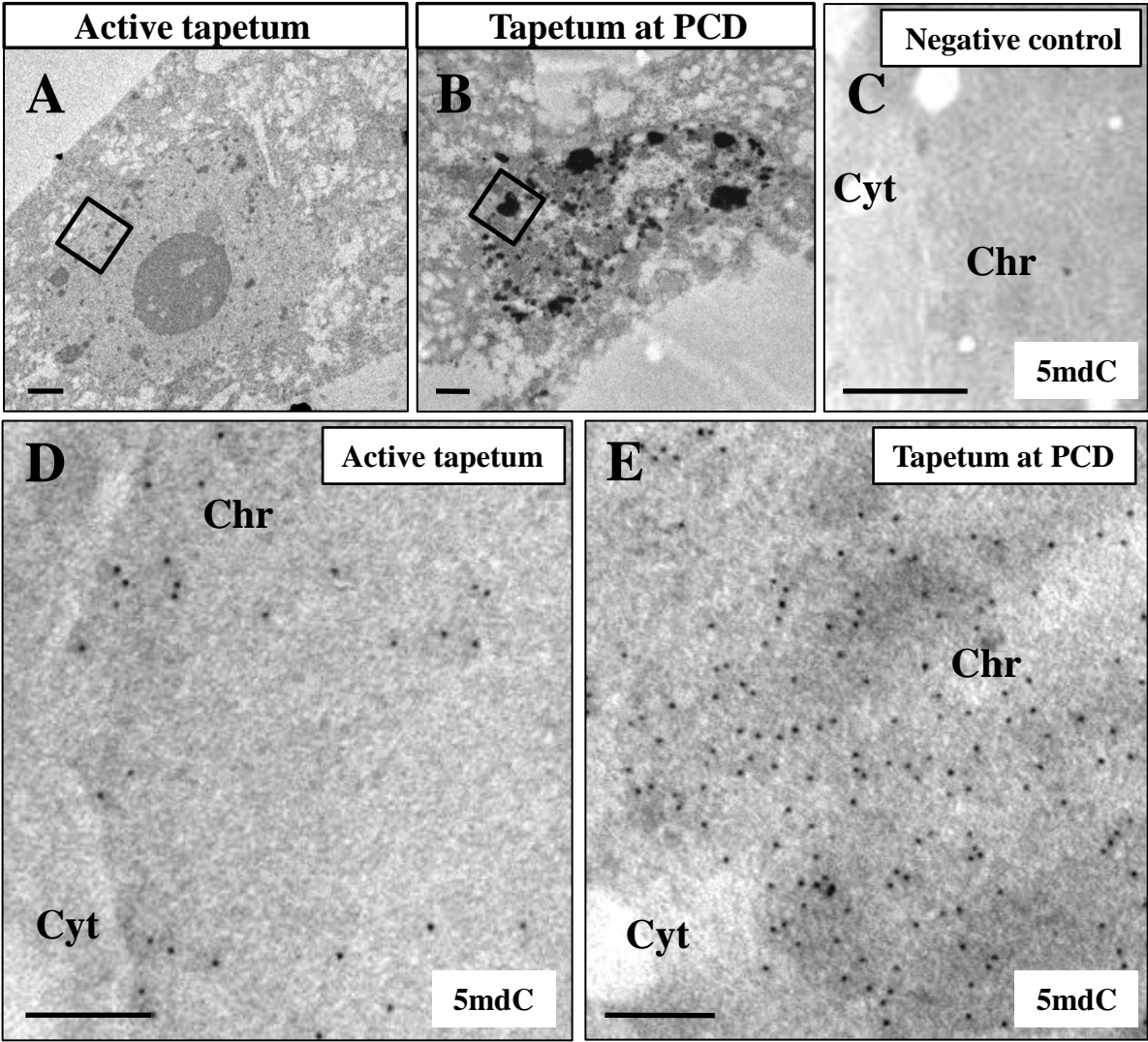


Figure 7

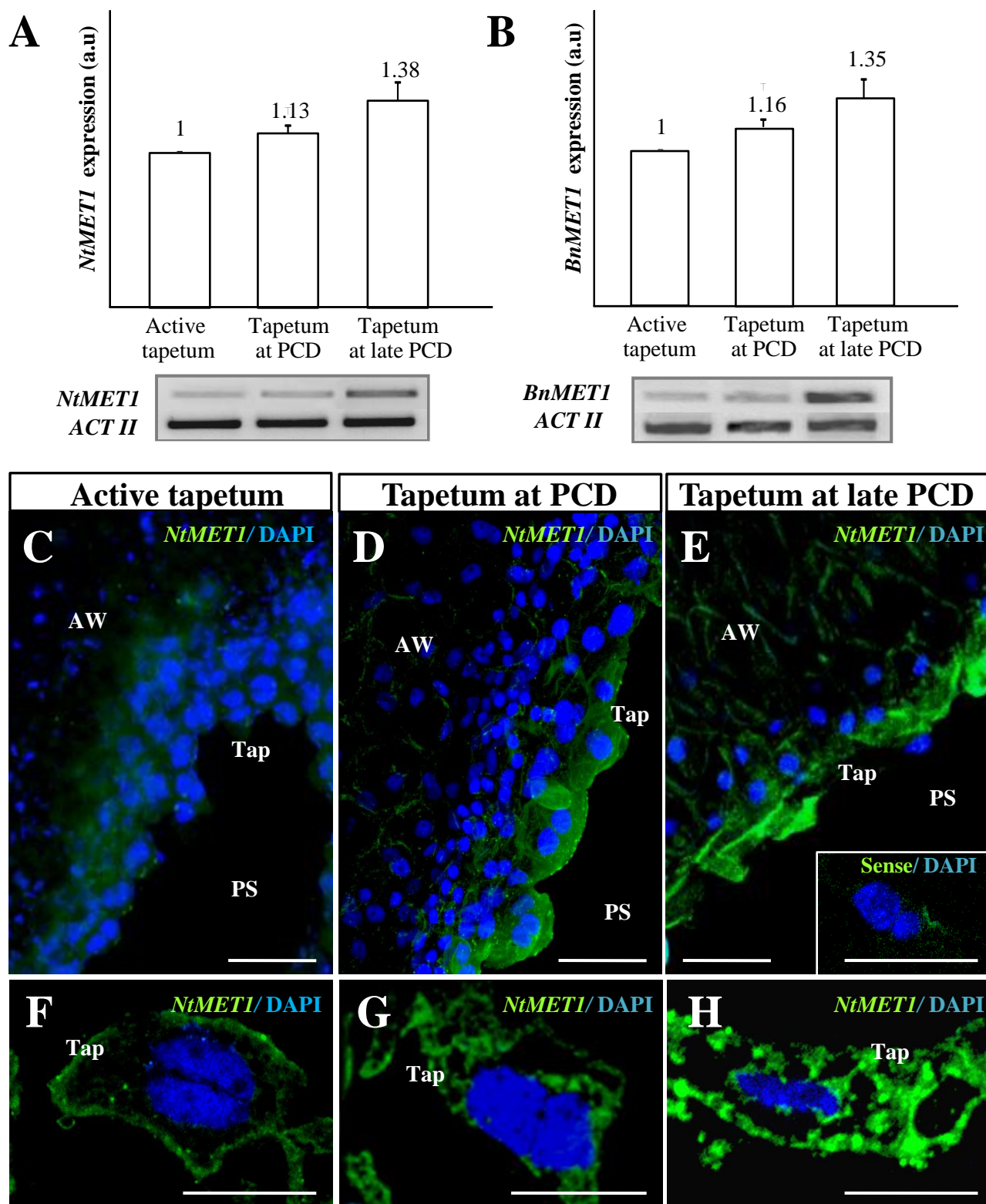



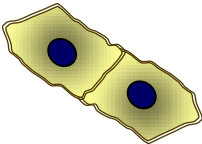
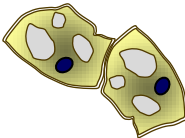



Figure 8

Pollen developmental stage		
Young microspore	Vacuolated microspore	Young pollen
		
Tapetum developmental stage		
Active tapetum	Tapetum at PCD	Tapetum at late PCD
		
+	++	+++
+	++	+++
+	++	+++
-	++	
+	++	++